IEEE Access
Multidisciplinary | Rapid Review | Open Access Journal

Received June 27, 2020, accepted July 6, 2020, date of publication July 9, 2020, date of current version July 23, 2020.

Digital Object Identifier 10.1109/ACCESS.2020.3008152

Robust Adaptive Sliding-Mode Control of a Permanent Magnetic Spherical Actuator With Delay Compensation

XIWEN GUO[1,2,3], KAIDA PAN[1,2], QUNJING WANG[1,2,3], AND YAN WEN[1,2]

[1]School of Electrical Engineering and Automation, Anhui University, Hefei 230601, China
[2]National Engineering Laboratory of Energy-saving Motor & Control Technique, Anhui University, Hefei 230601, China
[3]Engineering Research Center of Power Quality, Ministry of Education, Anhui University, Hefei 230601, China

Corresponding author: Xiwen Guo (xwguo2008@126.com)

This work was supported in part by the National Natural Science Foundation of China under Grant 51637001 and Grant 51307001, in part by the Natural Science Foundation of Anhui Province under Grant 2008085ME156, in part by the Young Core Teacher Program of Anhui University under Grant J01005126, and in part by the Academic and Technology Leaders Introduction Project of Anhui University under Grant 02303203(32030049).

ABSTRACT This study proposes an adaptive robust sliding-mode control strategy with time delay compensation to address the issues of the inaccuracy of modeling, friction, uncertain disturbances, and time delay in a permanent magnet spherical actuator trajectory tracking control system. First, an improved linear predictor is designed to compensate for the time delay in position information. Second, a robust sliding mode controller is designed to suppress the influence of uncertain disturbance. Third, the constant parameters of the spherical actuator are estimated using the adaptive law and compensated at the control input. The stability of the adaptive robust sliding-mode controller is proved by the Lyapunov theorem. Simulation and experimental results show that the control strategy proposed in this research has good dynamic and static performance, which can provide reference for the further engineering application of multi-degree of freedom control system.

INDEX TERMS Adaptive control, delay compensation, linear predictor, permanent magnet spherical actuator, robust sliding mode control, trajectory tracking.

I. INTRODUCTION

A permanent magnet spherical actuator (PMSA) has the advantages of compact structure, relatively large range of motion and rapid dynamic response. Given that the PMSA can provide three degree-of-freedom movement in one joint, this system is used in various applications in modern aerospace, robotics and other fields [1]–[3].

However, PMSA is a typical multivariable, coupled, and time-varying nonlinear system. The difficulties and challenges of PMSA control include inaccuracy of modeling, friction, uncertain disturbances, and time delay. Centripetal and Coriolis forces, friction, and uncertain disturbances directly interrupt the output torque, thereby possibly causing the rotor to perform unintended movements. Without delay compensation, the position and speed data used by the controller would be outdated. Therefore, the controller would calculate the output torque based on inaccurate data, which would not suit the current position.

In recent years, numerous studies have been conducted to solve the preceding problems. References [4], [5] proposed to apply the classical proportional plus derivative (PD) control to the PMSA control system. Although the design of the PD control system is simple and easy to realize, it is vulnerable to uncertainties and uncertain disturbances, thereby causing large steady-state errors. Reference [6] used calculation torque method to control the spherical actuator, thereby relatively realizing decoupling control. However, the scheme is based on an accurate dynamic model, in which the control accuracy will be considerably affected by model inaccuracy, friction, and uncertain disturbance. In references [7], [8], a neural network capable of self-learning is used to compensate for model inaccuracy and the influence of uncertain disturbance, thereby improving the control accuracy.

The associate editor coordinating the review of this manuscript and approving it for publication was Ahmed A. Zaki Diab.

However, the heavy computation of the algorithm and possibility of falling in the local optimal solution, have resulted in the difficulty of the neural network control system to meet the requirements of real-time control and practical applications. Reference [9], [10] used extended observer to compensate for the disturbance by merging the cross-channel interference into lumped disturbance. However, the selection of the parameters and nonlinear functions limits its application in the PMSA control. References [11], [12] combined robust control and sliding-mode control because the latter has such features as simple structure, fast response, strong robustness to uncertain interference and parameter perturbation. A robust controller with fixed structure and parameters is used to ensure that the system is stable under the worst condition. However, this control strategy cannot compensate for the disturbance from the input of the controller, but merely reduces the error caused by the disturbance. Thus, accuracy is not guaranteed. References [13]–[15] combined, the robust sliding mode control with adaptive control and disturbance observer to compensate for the errors caused by modeling inaccuracy and friction in the control input. The upper bound of the uncertain disturbance is reduced and the control performance is improved.

By contrast, the digital control system of PMSA has experienced delay caused by heavy computation. Previous PMSA control schemes have disregarded digital system delay or merely use robust control or disturbance observer to compensate for the errors caused by the delay as uncertain disturbance. However, the position information used by the controller is still from the past, which is not the same as the present position information. Thus, the accurate trajectory tracking control cannot be realized. Aiming at the delay problem of the digital control system, references [16], [17] proposed solutions through the Smith predictor and state observer, respectively, but Smith predictor and state observer need an accurate dynamic model. Only when the control object and the dynamic model are completely matched, can good control performance be achieved. The preceding model-based delay compensation method is not applicable because of the difficulty in establishing an accurate dynamic model for the permanent magnet spherical actuator control system. To avoid dependence on the dynamic model, some delay compensation methods that are independent of the model are proposed. In reference [18], time delay is reduced by changing the digital sampling moment. Given that the applicable requirement of this method is that the computation time of the control algorithm is less than the sampling period, this method is not suitable for the control system of PMSA. In references [19], [20], the first-order digital filter and the second-order digital filter are used to reduce the time delay respectively. However, this compensation method can amplify the measurement noise near the Nyquist frequency, thereby necessitating additional filters. In references [21], [22], an adaptive fuzzy predictor is proposed to compensate for the time delay. This compensation method can estimate the future values of the system states with an unknown time delay of known bound. In reference [23], a robust H infinity output feedback controller is developed to deal with the problem of active suspension control with actuator faults and unknown time delay. The time delay of the PMSA system can be approximated as a constant and measured through experiments. Thus, a compensation method maximizes the known time delay that would considerably suit the PMSA system. In references [24], [25], a linear predictor (LP) is proposed to predict control variables by linear extrapolation. The computation amount of this method is small, which is suitable for online prediction. Moreover, this method uses a time delay constant to predict the future states of the system. LP can also improve the controller bandwidth. However, the prediction accuracy of the LP is reduced when the signal frequency goes up, thereby resulting in an unsatisfied delay compensation performance [26]. The motivation of the current study is to develop a control strategy that can address the inaccuracy of modelling, friction, uncertain disturbances and time delay. Therefore, this study proposes an adaptive sliding mode robust controller with modified LP, which combines the advantages of adaptive controller, sliding-mode control, and LP: (1) The adaptive controller can estimate the constant parameter of PMSA, which is needed to compensate for the centripetal and Coriolis forces. (2) The sliding-mode controller is used to deal with friction and uncertain disturbances. (3) Lastly, the LP is used to predict the position data, thereby compensating for the time delay.

The remainder of this paper is organized as follows. Section II introduces the structure and dynamic model of PMSA. Section III proposes the delay compensation method and provides a digital example. Section IV designs an adaptive robust sliding mode controller and proves its stability. Section V and VI present the simulation and experiment results, and it shows that the proposed control strategy can ensure that the PMSA control system has good tracking performance in the presence of inaccuracy modeling, friction, uncertain disturbance and computation delay.

II. STRUCTURE AND DYNAMIC MODEL OF PMSA

A. PMSA STRUCTURE

The PMSA structure in this research is shown in Fig. 1. PMSA comprise the rotor, stator shell, permanent magnets, coils, and output shaft. The rotor is embedded with a 4-layer of 10 equally spaced Nd-Fe-B permanent magnets. The adjacent magnets have opposite polarities. The stator houses 2-layer of 12 equally spaced air-core coils.

The superposition principle, states that when the stator coil of PMSA is electrified according to a certain electrifying strategy, the electromagnetic torque is generated between the stator coil and rotor permanent magnet. Thereafter, the three-degree-of-freedom motions of rotation, yaw, and pitch are realized.

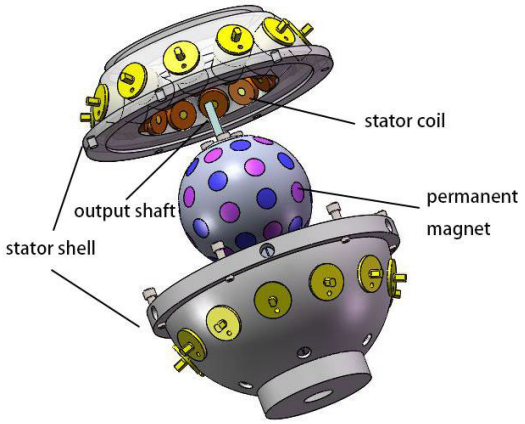

FIGURE 1. PMSA Structure.

B. DYNAMIC MODEL OF THE PMSA

Considering friction and uncertain disturbance of PMSA, a Lagrange formulation of the PMSA control system in terms of the Cardan angles coordinates is established as follows:

$$\boldsymbol{J}(\boldsymbol{q})\ddot{\boldsymbol{q}} + \boldsymbol{C}(\boldsymbol{q},\dot{\boldsymbol{q}})\dot{\boldsymbol{q}} + \boldsymbol{f}(\dot{\boldsymbol{q}}) = \boldsymbol{\tau} \tag{1}$$

where

$$\boldsymbol{J}(\boldsymbol{q}) = \begin{bmatrix} \mathrm{J_{dq}}\cos^2\beta + \mathrm{J_p}\sin^2\beta & 0 & \mathrm{J_p}\sin\beta \\ 0 & \mathrm{J_{dq}} & 0 \\ \mathrm{J_p}\sin\beta & 0 & \mathrm{J_p} \end{bmatrix} \tag{2}$$

$$\boldsymbol{C}(\boldsymbol{q},\dot{\boldsymbol{q}}) = \begin{bmatrix} C_{11} & C_{12} & C_{13} \\ C_{21} & C_{22} & C_{23} \\ C_{31} & C_{32} & C_{33} \end{bmatrix} \tag{3}$$

$$\begin{cases} C_{11} = (\mathrm{J_p} - \mathrm{J_{dq}})\dot{\beta} sin\beta cos\beta \\ C_{12} = (\mathrm{J_p} - \mathrm{J_{dq}})\dot{\alpha} sin\beta cos\beta \\ C_{13} = \mathrm{J_p}\dot{\beta} cos\beta \\ C_{21} = (\mathrm{J_{dq}} - \mathrm{J_p})\dot{\alpha} sin\beta cos\beta \\ C_{22} = 0 \\ C_{23} = \mathrm{J_p}\dot{\alpha} cos\beta \\ C_{31} = 0 \\ C_{32} = \mathrm{J_p}\dot{\alpha} cos\beta \\ C_{33} = 0 \end{cases} \tag{4}$$

where $\boldsymbol{q} = [\alpha, \beta, \gamma]^T$ and $\boldsymbol{q}$ is the rotor orientation represented with Cardan angles; $\boldsymbol{J}(\boldsymbol{q}) \in R^3$ denotes the symmetric, bounded, and positive definite inertia matrix; $\boldsymbol{C}(\boldsymbol{q},\dot{\boldsymbol{q}})$ represents the matrix of the centripetal and Coriolis forces; $\boldsymbol{f}(\dot{\boldsymbol{q}}) \in R^3$ is the vector of the general disturbances including friction and uncertain disturbances; $\boldsymbol{\tau}$ is the vector of the control input torque; and $\mathrm{J_{dq}}$ and $\mathrm{J_p}$ denote the moment of inertia of the rotation around the d, q, and p axes respectively. The symmetric structure of the PMSA results in $\mathrm{J_d}$=$\mathrm{J_q}$ = $\mathrm{J_{dq}}$.

III. TIME DELAY COMPENSATION

A. TIME DELAY IN PMSA CONTROL SYSTEM

The heavy computation of the PMSA electrifying strategy causes a time delay in the control system. Reference [27] proposed to use different coil combinations to avoid or reduce calculations caused by simultaneously electrifying all coils. However, this method is an open-loop control, which is not suitable for the closed-loop PMSA trajectory tracking system. The current optimization strategy proposed in reference [28] can reduce the number of simultaneously electrified coils, although this process entails heavy computation. The electrifying strategy of the PMSA closed-loop control system in the current study is based on the torque calculation method proposed in reference [29]. Accordingly, the torque characteristic model of a single stator coil and single rotor permanent magnet should be established. When several groups of stator coils are electrified, the electromagnetic torque vector can be considered as a combination of separate torque generated by each coil and permanent magnet. The combined torque vector can be expressed as follows:

$$\begin{aligned} \boldsymbol{T} &= \begin{bmatrix} T_X \\ T_Y \\ T_Z \end{bmatrix} = \sum_{i=1}^{n}\sum_{j=1}^{m} F(q)\frac{\boldsymbol{s}_{\mathrm{ri}} \times \boldsymbol{s}_{\mathrm{sj}}}{\left|\boldsymbol{s}_{\mathrm{ri}} \times \boldsymbol{s}_{\mathrm{sj}}\right|}\mathrm{N}i \\ &= \begin{bmatrix} f_{\mathrm{X1}} & f_{\mathrm{X2}}\cdots & f_{\mathrm{Xm}} \\ f_{\mathrm{Y1}} & f_{\mathrm{Y2}}\cdots & f_{\mathrm{Ym}} \\ f_{\mathrm{Z1}} & f_{\mathrm{Z2}}\cdots & f_{\mathrm{Zm}} \end{bmatrix} \cdot \begin{bmatrix} I_1 \\ I_2 \\ \vdots \\ I_m \end{bmatrix} = \boldsymbol{A}\cdot\boldsymbol{I} \end{aligned} \tag{5}$$

where $\boldsymbol{s}_{ri}, \boldsymbol{s}_{\mathrm{rj}}$ is the position vector of the rotor permanent magnet and stator coil, respectively; N is the number of turns of the coil; $\boldsymbol{F}(\boldsymbol{q})$ is the torque generated by a single coil and single permanent magnet; $\boldsymbol{f}_{\mathrm{Xi}}, \boldsymbol{f}_{\mathrm{Yi}}, \boldsymbol{f}_{\mathrm{Zi}}$ are the torque components in the X, Y, Z directions, respectively, of Cartesian coordinate system generated by the i th coil under unit positive current; and $\boldsymbol{I}_i$ is the current of the i th coil.

Based on the torque vector model $\boldsymbol{T}$, the control current of the stator coil can be obtained through $\boldsymbol{A}^+$,which is the pseudo-inverse matrix of $\boldsymbol{A}$, as follows:

$$\boldsymbol{I} = \boldsymbol{A}^+\boldsymbol{T} \tag{6}$$

Equation (5) shows that this electrifying strategy requires heavy computation. An example is the PMSA in this study. The motor consists of 24 stator coils and 40 rotor permanent magnets. Therefore, 960 times of calculation are needed. In addition, the pseudo inverse matrix $\boldsymbol{A}^+$ should be solved. Although this method requires extensive of calculation, it can cover all the working conditions of the spherical actuator and is markedly suitable for the closed-loop tracking of the complex trajectory. A certain amount of time is needed for calculation in the digital control system and in the data transmission of sensors and driving circuits. The control torque is calculated according to the position information acquired before the system time delay. Thus, the output torque is delayed, thereby degrading the control system performance.

B. DELAY COMPENSATION METHOD

The delay of the PMSA control system mainly exists in the calculation process of the controller. When the hardware condition of the controller is fixed, the value of the delay can be approximately regarded as a measurable constant.

The position of PMSA is set at a certain time as $\boldsymbol{q}(t)$ and the speed as $\dot{\boldsymbol{q}}(t)$. At this moment, the delayed position information in the controller is $\boldsymbol{q}(t - \mathrm{t_d})$ and the delayed speed signal is $\dot{\boldsymbol{q}}(t - \mathrm{t_d})$. If $\mathrm{t_d}$ is relatively small, then the following approximate equation holds:

$$\frac{\boldsymbol{q}(t) - \boldsymbol{q}(t - \mathrm{t_d})}{\mathrm{t_d}} \approx \dot{\boldsymbol{q}}(t - \mathrm{t_d}) \tag{7}$$

Thus,

$$\boldsymbol{q}(t) \approx \dot{\boldsymbol{q}}(t - t_d)\, t_d + \boldsymbol{q}(t - t_d) \tag{8}$$

The predicted position signal $\boldsymbol{q}_\mathrm{p}$ is defined as follows:

$$\boldsymbol{q}_p = \dot{\boldsymbol{q}}(t - t_d)\, t_d + \boldsymbol{q}(t - t_d) \tag{9}$$

The speed signal $\dot{\boldsymbol{q}}(t - \mathrm{t_d})$ used in the preceding linear prediction method is the signal after delay and the PMSA speed is changing continuously in the delay process. Thus, the speed signal should be compensated. If $\mathrm{t_d}$ is relatively small, then the following approximate equation holds:

$$\frac{\dot{\boldsymbol{q}}(t) - \dot{\boldsymbol{q}}(t - \mathrm{t_d})}{\mathrm{t_d}} \approx \frac{\dot{\boldsymbol{q}}(t - \mathrm{t_d}) - \dot{\boldsymbol{q}}(t - 2\mathrm{t_d})}{\mathrm{t_d}} \tag{10}$$

The average speed $\dot{\boldsymbol{q}}_\mathrm{a}$ during the delay can be obtained by the following approximate equation:

$$\dot{\boldsymbol{q}}_a \approx \dot{\boldsymbol{q}}(t - \mathrm{t_d}) + (\dot{\boldsymbol{q}}(t - \mathrm{t_d}) - \dot{\boldsymbol{q}}(t - 2\mathrm{t_d}))/2 \tag{11}$$

The compensated predicted speed signal $\dot{\boldsymbol{q}}_\mathrm{p}$ is defined as follows:

$$\dot{\boldsymbol{q}}_\mathrm{p} = \dot{\boldsymbol{q}}(t - \mathrm{t_d}) + (\dot{\boldsymbol{q}}(t - \mathrm{t_d}) - \dot{\boldsymbol{q}}(t - 2\mathrm{t_d}))/2 \tag{12}$$

By replacing $\dot{\boldsymbol{q}}(t - \mathrm{t_d})$ in (8) with $\boldsymbol{q}_\mathrm{p}$ in (12), the compensated position signal $\boldsymbol{q}_\mathrm{com}$ can be obtained as follows:

$$\boldsymbol{q}_\mathrm{com} = \boldsymbol{q}(t - \mathrm{t_d}) + \dot{\boldsymbol{q}}_\mathrm{p}\mathrm{t_d} \tag{13}$$

The transfer function of $\boldsymbol{q}_\mathrm{com}$ is defined as $\boldsymbol{q}_\mathrm{com}(S)$, and $\boldsymbol{q}_\mathrm{p}$ as $\boldsymbol{q}_\mathrm{p}(S)$. The delay and compensation processes can be expressed by transfer function as $\boldsymbol{q}_\mathrm{com}(S)\mathrm{e}^{-\mathrm{t_d}S}$, $\boldsymbol{q}_\mathrm{p}(S)\mathrm{e}^{-\mathrm{t_d}S}$. Fig. 2 shows the bode gram of the two transfer functions. Meanwhile, $\mathrm{t_d}$ in these functions are set to 0.022 sec, which is the measured time delay constant of the PMSA system used in this study. The bode gram shows that the proposed predictor has less phase lag for high-frequency signal than the normal LP.

C. NUMERICAL EXAMPLE

The following signal is used as an example:

$$\begin{cases} \boldsymbol{q}(t) = \sin(t), & t > 0 \\ \boldsymbol{q}(t) = 0, & t \le 0 \end{cases} \tag{14}$$

The delay time $\mathrm{t_d}$ is set at 0.2 sec. Given that every output signal of the digital control system of PMSA must take $\mathrm{t_d}$, the computation frequency of the digital system can be considered as $1/\mathrm{t_d}$.

In Fig. 3, $\boldsymbol{q}$ is the actual position signal, $\boldsymbol{q}_\mathrm{d}$ is the delayed position signal, $\boldsymbol{q}_\mathrm{p}$ is the prediction of position signal based on (9), and $\boldsymbol{q}_\mathrm{com}$ is the prediction of position signal based on (13).

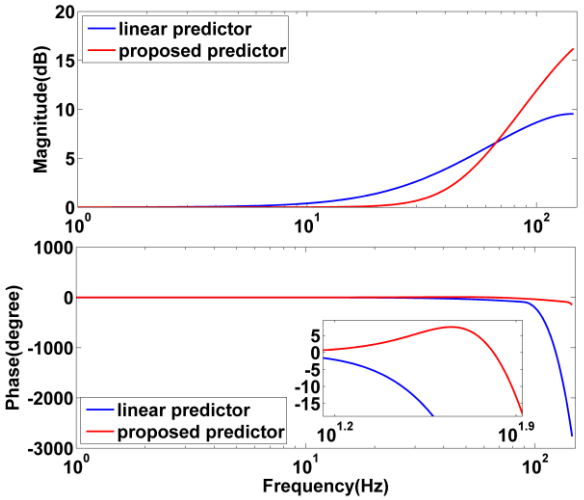

FIGURE 2. Bode gram of $\boldsymbol{q}_\mathrm{com}(S)\mathrm{e}^{-\mathrm{t_d}S}$, $\boldsymbol{q}_\mathrm{p}(S)\mathrm{e}^{-\mathrm{t_d}S}$.

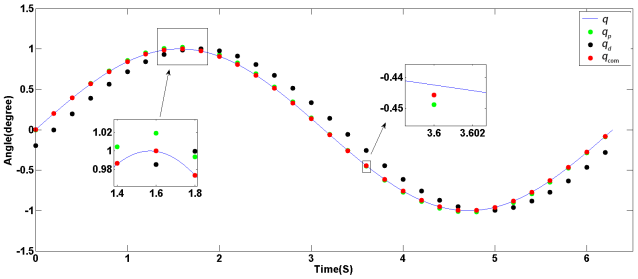

FIGURE 3. Trajectories of signals q, q_d, q_p, and q_com for the numerical example.

The numerical example shows that the proposed position prediction method can make the position information given to the controller closer to the actual position signal $\boldsymbol{q}$ without delay. When the speed changes rapidly, the error of the LP with speed compensation is smaller than the one without speed compensation. Although the position signal in the actual control process may be more complex, the main goal of the proposed prediction method is able to improve the robustness of the PMSA control system for time delay.

IV. CONTROLLER DESIGN AND STABILITY ANALYSIS

A. DESIGN OF THE SLIDING-MODE CONTROLLER

The following sliding-mode controller is designed to suppress the influence of friction and uncertain disturbance on the control performance of PMSA:

$$\begin{cases} \boldsymbol{E}_q = \boldsymbol{q}_\mathrm{com} - \boldsymbol{q}_\mathrm{des} \\ \boldsymbol{S} = \dot{\boldsymbol{E}}_q + \boldsymbol{\Lambda}\boldsymbol{E}_q \end{cases} \tag{15}$$

where $\boldsymbol{q}_\mathrm{des}$ is the desired angle signal, $\boldsymbol{E}_q$ is the position error, $\boldsymbol{S}$ is the sliding face function, and $\boldsymbol{\Lambda}$ is a positive constant diagonal matrix.

The sliding-mode controller $\boldsymbol{u}_s$ satisfies the following relationship:

$$\frac{1}{2}\frac{\mathrm{d}}{\mathrm{d}t}\boldsymbol{S}^2 \leq -\eta\,|\boldsymbol{S}| \tag{16}$$

which ensures that the system state eventually converges to the sliding surface $\boldsymbol{S} = 0$. When the system state enters the sliding surface, such a state is determined by the linear differential equation $0 = \dot{E}_q\,\boldsymbol{\mathcal{C}}\,\boldsymbol{\Lambda}\boldsymbol{E}_q$, which ensures that the position error can converge to 0 when time tends to ∞. Given the uncertain disturbance in the control system, the output of the sliding-mode controller is taken as follows:

$$\begin{cases} \boldsymbol{u}_s = \boldsymbol{u}_{s1} + \boldsymbol{u}_{s2} \\ \boldsymbol{u}_{s1} = -\mathrm{k_s}\boldsymbol{S} \\ \boldsymbol{u}_{s2} = -\boldsymbol{\kappa}\,\mathrm{sgn}\,(\boldsymbol{S}) \\ \boldsymbol{\kappa} = [\mathrm{k}_1, \mathrm{k}_2, \mathrm{k}_3]^{\mathrm{T}} \\ \boldsymbol{\kappa} = \sup|\boldsymbol{f}\,(\dot{\boldsymbol{q}})| \end{cases} \tag{17}$$

where $\boldsymbol{u}_{s1}$ is the feedback term; $\boldsymbol{u}_{s2}$ is the robust term; $\mathrm{k_s}, \mathrm{k}_1, \mathrm{k}_2, \mathrm{k}_3$ are positive constants; $\mathrm{k_s}$ determines the convergence speed of the error on the sliding surface; and $\boldsymbol{\kappa}$ is the gains of the robust term, which are the upper bounds of the uncertain disturbances.

B. DESIGN OF ADAPTIVE CONTROLLER

To compensate for the Coriolis and centrifugal forces, an adaptive controller is designed to estimate the moment of inertia $\mathrm{J_p}, \mathrm{J_{dq}}$ of PMSA's dynamic model which are two constant parameters.

Define

$$\boldsymbol{q}_{\mathrm{r}} = \dot{\boldsymbol{q}}_{\mathrm{des}} - \boldsymbol{\Lambda}\boldsymbol{E}_q \tag{18}$$

Substitute (18) into (15) and obtain

$$\boldsymbol{S} = \dot{\boldsymbol{q}}_{\mathrm{com}} - \dot{\boldsymbol{q}}_{\mathrm{r}} \tag{19}$$

$$\dot{\boldsymbol{S}} = \ddot{\boldsymbol{q}}_{\mathrm{com}} - \ddot{\boldsymbol{q}}_{\mathrm{r}} \tag{20}$$

$$\boldsymbol{J}\dot{\boldsymbol{S}} = \boldsymbol{J}(\ddot{\boldsymbol{q}}_{\mathrm{com}} - \ddot{\boldsymbol{q}}_{\mathrm{r}}) = \tau - \boldsymbol{C}\dot{\boldsymbol{q}}_{\mathrm{com}} - \boldsymbol{J}\ddot{\boldsymbol{q}}_{\mathrm{r}} - f(\dot{\boldsymbol{q}}_{\mathrm{com}}) \tag{21}$$

Define

$$\boldsymbol{C}\dot{\boldsymbol{q}}_{\mathrm{com}} + \boldsymbol{J}\ddot{\boldsymbol{q}}_{\mathrm{com}} = \boldsymbol{Y}(\boldsymbol{q}_{\mathrm{com}}, \dot{\boldsymbol{q}}_{\mathrm{com}}, \dot{\boldsymbol{q}}_{\mathrm{r}}, \ddot{\boldsymbol{q}}_{\mathrm{r}})\boldsymbol{a}(\mathrm{J_p}, \mathrm{J_{dq}}) \tag{22}$$

where $\boldsymbol{Y}(\boldsymbol{q}_{\mathrm{com}}, \dot{\boldsymbol{q}}_{\mathrm{com}}, \dot{\boldsymbol{q}}_{\mathrm{r}}, \ddot{\boldsymbol{q}}_{\mathrm{r}})$ is a function independent of the unknown constant parameters of the dynamic equations (2), (3), and (4); and $\boldsymbol{a}(\mathrm{J_p}, \mathrm{J_{dq}})$ is a constant matrix consisting of the unknown constant parameter.

Define

$$\hat{\boldsymbol{a}} - \boldsymbol{a}\left(\mathrm{J_p}, \mathrm{J_{dq}}\right) = \tilde{\boldsymbol{a}}. \tag{23}$$

where $\tilde{\boldsymbol{a}}$ is the error of the adaptive parameters and $\hat{\boldsymbol{a}}$ is the estimated parameter.

Adaptive law is chosen as follows:

$$\dot{\hat{\boldsymbol{a}}} = -\boldsymbol{P}\boldsymbol{Y}^{T}\left(\boldsymbol{q}, \dot{\boldsymbol{q}}, \dot{\boldsymbol{q}}_{\mathrm{r}}, \ddot{\boldsymbol{q}}_{\mathrm{r}}\right)\boldsymbol{S}, \tag{24}$$

where $\boldsymbol{P}$ is a symmetric positive constant matrix. The output of the adaptive controller is as follows:

$$\boldsymbol{u}_{\boldsymbol{a}} = \hat{\boldsymbol{J}}\ddot{\boldsymbol{q}}_{\mathrm{r}} + \hat{\boldsymbol{C}}\dot{\boldsymbol{q}}_{\mathrm{r}} \tag{25}$$

C. STABILITY ANALYSIS

The output of the controller is as follows:

$$\boldsymbol{\tau} = \boldsymbol{u}_s + \boldsymbol{u}_{\boldsymbol{a}} \tag{26}$$

A Lyapunov candidate is chosen as follows

$$\boldsymbol{V}\,(t) = \frac{1}{2}\boldsymbol{S}^{\mathrm{T}}\boldsymbol{J}\boldsymbol{S} + \frac{1}{2}\tilde{\boldsymbol{a}}^{\mathrm{T}}\boldsymbol{P}^{-1}\tilde{\boldsymbol{a}} \tag{27}$$

The derivation is expressed as follows:

$$\dot{\boldsymbol{V}}\,(t) = \boldsymbol{S}^{\mathrm{T}}\boldsymbol{J}\dot{\boldsymbol{S}} + \frac{1}{2}\boldsymbol{S}^{\mathrm{T}}\dot{\boldsymbol{J}}\boldsymbol{S} + \tilde{\boldsymbol{a}}^{\mathrm{T}}\boldsymbol{P}^{-1}\dot{\tilde{\boldsymbol{a}}} \tag{28}$$

By using (1), (15), (17), (21), (24), and (26), Equation (28) is further deduced as follows:

$$\begin{aligned}
\dot{\boldsymbol{V}}\,(t) &= \boldsymbol{S}^{\mathrm{T}}\left(\boldsymbol{\tau} - \boldsymbol{C}\dot{\boldsymbol{q}}_{\mathrm{com}} - \boldsymbol{J}\ddot{\boldsymbol{q}}_{\mathrm{r}} - \boldsymbol{f}\left(\dot{\boldsymbol{q}}_{\mathrm{com}}\right)\right) \\
&\quad + \frac{1}{2}\boldsymbol{S}^{\mathrm{T}}\dot{\boldsymbol{J}}\boldsymbol{S} + \tilde{\boldsymbol{a}}^{\mathrm{T}}\mathbf{P}^{-1}\dot{\tilde{\boldsymbol{a}}} \\
&= \boldsymbol{S}^{\mathrm{T}}\left(\boldsymbol{\tau} - \boldsymbol{C}\left(\boldsymbol{s} + \dot{\boldsymbol{q}}_{\mathrm{r}}\right) - \boldsymbol{J}\ddot{\boldsymbol{q}}_{\mathrm{r}} - \boldsymbol{f}\left(\dot{\boldsymbol{q}}_{\mathrm{com}}\right)\right) \\
&\quad + \frac{1}{2}\boldsymbol{S}^{\mathrm{T}}\dot{\boldsymbol{J}}\boldsymbol{S} + \tilde{\boldsymbol{a}}^{\mathrm{T}}\mathbf{P}^{-1}\dot{\tilde{\boldsymbol{a}}} \\
&= \boldsymbol{S}^{\mathrm{T}}\left(-\boldsymbol{k}_s\boldsymbol{S} + \widehat{\boldsymbol{J}}\ddot{\boldsymbol{q}}_{\mathrm{r}} + \widehat{\boldsymbol{C}}\dot{\boldsymbol{q}}_{\mathrm{r}} - \boldsymbol{C}\left(\boldsymbol{s} + \dot{\boldsymbol{q}}_{\mathrm{r}}\right) - \boldsymbol{J}\ddot{\boldsymbol{q}}_{\mathrm{r}}\right) \\
&\quad + \frac{1}{2}\boldsymbol{S}^{\mathrm{T}}\dot{\boldsymbol{J}}\boldsymbol{S} + \tilde{\boldsymbol{a}}^{\mathrm{T}}\mathbf{P}^{-1}\dot{\tilde{\boldsymbol{a}}} - \boldsymbol{S}^{\mathrm{T}}\left(\boldsymbol{f}\left(\dot{\boldsymbol{q}}_{\mathrm{com}}\right) + \boldsymbol{\kappa}\,\mathrm{sgn}\,(\boldsymbol{S})\right) \\
&= \boldsymbol{S}^{\mathrm{T}}\left(-\boldsymbol{k}_s\boldsymbol{S} + \dot{\boldsymbol{J}}\ddot{\boldsymbol{q}}_{\mathrm{r}} + \widehat{\boldsymbol{C}}\dot{\boldsymbol{q}}_{\mathrm{r}} - \boldsymbol{C}\boldsymbol{S}\right) \\
&\quad + \frac{1}{2}\boldsymbol{S}^{\mathrm{T}}\dot{\boldsymbol{J}}\boldsymbol{S} + \tilde{\boldsymbol{a}}^{\mathrm{T}}\mathbf{P}^{-1}\dot{\tilde{\boldsymbol{a}}} - \boldsymbol{S}^{\mathrm{T}}\left(\boldsymbol{f}\left(\dot{\boldsymbol{q}}_{\mathrm{com}}\right) + \boldsymbol{\kappa}\,\mathrm{sgn}\,(\boldsymbol{S})\right) \\
&= -\boldsymbol{k}_s\boldsymbol{S}^{\mathrm{T}}\boldsymbol{S} + \boldsymbol{S}^{\boldsymbol{T}}\boldsymbol{Y}\tilde{\boldsymbol{a}} - \boldsymbol{S}^{\mathrm{T}}\left(\boldsymbol{f}\left(\dot{\boldsymbol{q}}_{\mathrm{com}}\right) + \boldsymbol{\kappa}\,\mathrm{sgn}\,(\boldsymbol{S})\right) \\
&\quad + \frac{1}{2}\boldsymbol{S}^{\mathrm{T}}\left(\dot{\boldsymbol{J}} - 2\boldsymbol{C}\right)\boldsymbol{S} + \tilde{\boldsymbol{a}}^{\mathrm{T}}\mathbf{P}^{-1}\dot{\tilde{\boldsymbol{a}}} \\
&= -\boldsymbol{k}_s\boldsymbol{S}^{\mathrm{T}}\boldsymbol{S} + \tilde{\boldsymbol{a}}^{\mathrm{T}}\left(\mathbf{P}^{-1}\dot{\tilde{\boldsymbol{a}}} + \boldsymbol{Y}^{\mathrm{T}}\boldsymbol{S}\right) \\
&\quad - \boldsymbol{S}^{\mathrm{T}}\left(\boldsymbol{f}\left(\dot{\boldsymbol{q}}_{\mathrm{com}}\right) + \boldsymbol{\kappa}\,\mathrm{sgn}\,(\boldsymbol{S})\right) \\
&= -\boldsymbol{k}_s\boldsymbol{S}^{\mathrm{T}}\boldsymbol{S} - \boldsymbol{S}^{\mathrm{T}}\left(\boldsymbol{f}\left(\dot{\boldsymbol{q}}_{\mathrm{com}}\right) + \boldsymbol{\kappa}\,\mathrm{sgn}\,(\boldsymbol{S})\right) \leq 0
\end{aligned} \tag{29}$$

The function $\dot{\boldsymbol{V}}(t)$ is negative semi-definite. Thus, the stability of the controller is proven according to Lasalle's invariant principle.

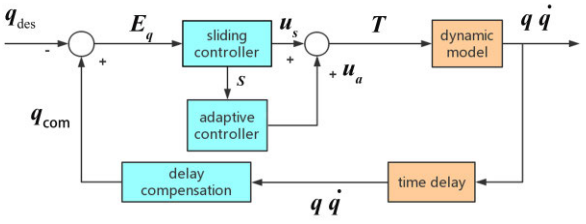

FIGURE 4. Structure of the PMSA control system.

D. STRUCTURE OF THE PMSA CONTROL SYSTEM

The block diagram of the PMSA control system is shown in Fig. 4, including the sliding-mode controller, adaptive controller, and delay compensation module. The delay compensation includes the electrifying strategy in (5) and (6).

V. SIMULATION AND ANALYSIS

The PMSA structure indicates that the dynamic simulation model is established in the automatic dynamic analysis of the mechanical system (ADAMS). The moment of inertia of d, q, and p axes of PMSA is obtained as follows:

$$\begin{cases} \mathrm{J_d} = \mathrm{J_q} = \mathrm{J_{dq}} = 0.01548 \left(\mathrm{kg \cdot m^2}\right) \\ \mathrm{J_p} = 0.01571 \left(\mathrm{kg \cdot m^2}\right) \end{cases} \tag{30}$$

The desired trajectory $\boldsymbol{q}_{\mathrm{des}}$ and initial state $\boldsymbol{q}(0)$ are as follows

$$\begin{cases} \boldsymbol{q}_{\mathrm{des}} = [15\sin(\pi t)\ ,\ 15\cos(\pi t)\ ,\ 15t/4] \\ \boldsymbol{q}(0) = [0, 0, 0] \end{cases} \tag{31}$$

This trajectory has a varying speed and different functions in each direction. The initial error of β direction is 15 degree. The results of the simulation can show controller's performance on complex trajectory with large initial error.

Friction is set to 0.02N and its direction is opposite to the movement direction of PMSA. Noted that the actual friction is considerably complex and other uncertain disturbances are present. The total uncertain disturbances are set as random numbers with normal distribution from 0 to 0.03. The parameters of the controller are set as follows:

$$\begin{cases} \boldsymbol{\Lambda} = \mathrm{diag}(0.1, 0.1, 0.1) \\ \mathrm{k}_s = 0.1 \\ \mathrm{K} = [0.06, 0.06, 0.06]^{\mathrm{T}} \\ \mathbf{P} = \mathrm{diag}(1, 1, 1), \end{cases} \tag{32}$$

where diag(·) is the diagonal matrix.

The parameter of the PD controller used in the simulation is as follows

$$\begin{cases} \mathrm{k_P} = -0.15 \\ \mathrm{k_D} = -0.35 \end{cases} \tag{33}$$

The delay constant $\mathrm{t_d} = 0.02$ and calculating frequency of the digital system to $1/\mathrm{t_d}$ are set. The simulation time is set to 4 sec.

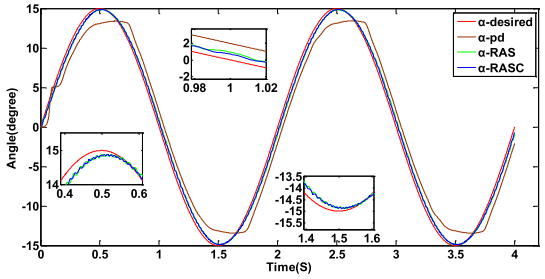

FIGURE 5. Position response to angle α.

The position response and tracking errors of the PD controller, adaptive sliding-mode robust controller (RAS) and adaptive sliding-mode robust controller with delay compensation (RASC) are shown in Figs. 5 to 7 and Figs. 8 to 10, respectively. Table 1 shows the mean square errors (MSEs) versus the different angles. The preceding simulation results

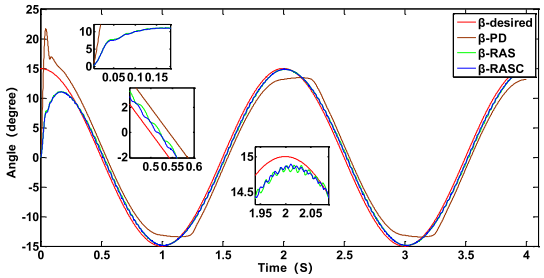

FIGURE 6. Position response to angle β.

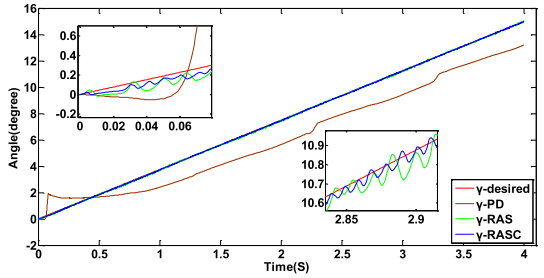

FIGURE 7. Position response to angle γ.

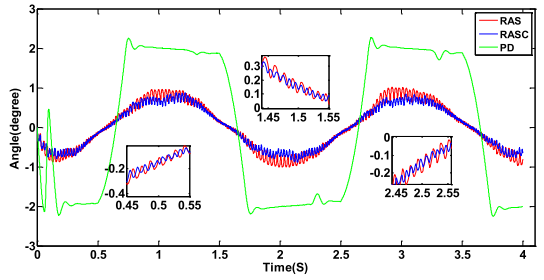

FIGURE 8. Tracking errors versus angle α.

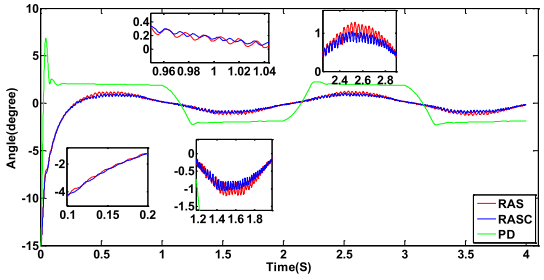

FIGURE 9. Tracking errors versus angle β.

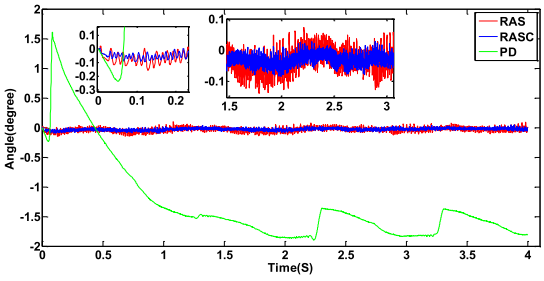

FIGURE 10. Tracking errors versus angle γ.

show that the proposed controller can effectively reduce the error caused by friction and uncertain disturbances and compensate for the Coriolis and centrifugal forces in the output

TABLE 1. Mean square errors versus the different angle.

Items	PD	RAS	RASC
Errors on angle α	3.2708	0.3711	0.2787
Errors on angle β	4.4661	2.7069	2.6218
Errors on angle γ	2.1716	0.0032	0.0014

torque. PMSA is controlled to track the desired trajectory. Compared with the PD controller, MSEs of RAS in the α, β, γ directions is decreased by 88.6%, 39.3%, and 99.8%, respectively. Compared with the RAS controller, the MSEs of RASC in α, β, γ directions are reduced by 24.8%, 3.1%, and 56.2%, respectively, after compensation. Compared with the PD controller, the RAS and RASC controllers respond to large initial error without overshoot, and the convergence rate of error is faster.

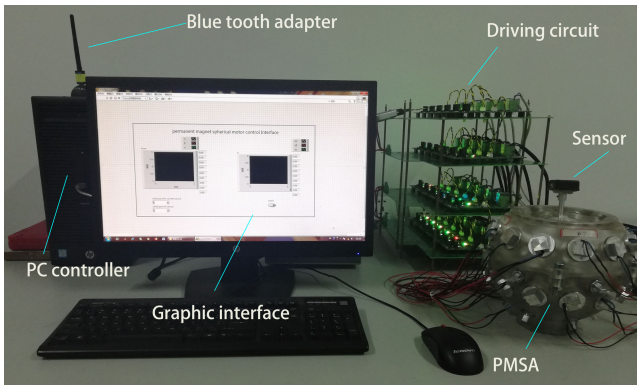

FIGURE 11. Experiment platform.

VI. EXPERIMENT AND ANALYSIS

The structure of the experimental platform is shown in Fig. 11. The detailed structure of PMSA used in this platform is described in Section II. A six-axis gyroscope position sensor is fixed on its output shaft through a flange, and can communicate with the controller through Bluetooth serial communication. The precision of the sensor is 0.05 degree.

The PC controller uses an i7-6700 processor. Through the graphical interface of the PC controller, users can edit the control parameters and select the desired trajectory. The driving circuit consists of 24 ARMs, each of which controls the current of a single coil of PMSA.

As shown in Fig. 12, after receiving the position information of PMSA, the controller calculates the corresponding torque using the proposed control strategy. The currents of the corresponding 24 coils can be obtained using (5) and (6). The current values will be sent to the drive circuit through serial port communication. Thereafter, the drive circuit passes the current into the stator coil of PMSA to generate electromagnetic torque that drives the rotor to track the desired trajectory.

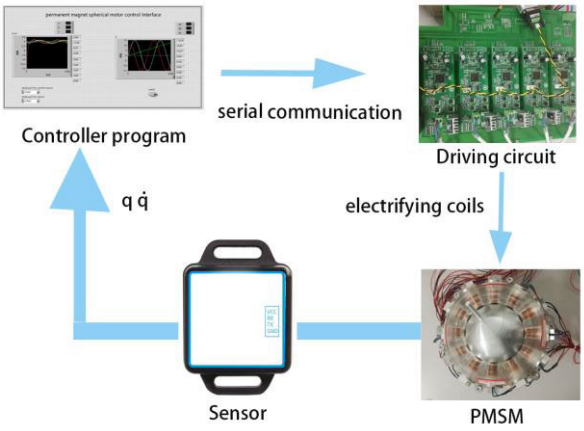

FIGURE 12. Schematic of the experiment platform.

The parameters of the controller, desired trajectory, and initial conditions used in the experiment are set to be the same as those of (30) and (31) in the simulation. The delay of the system is measured as 0.022±0.0002 sec, the calculating frequency of the digital system is 45.5 Hz, and the total experiment running time is set to 4 sec.

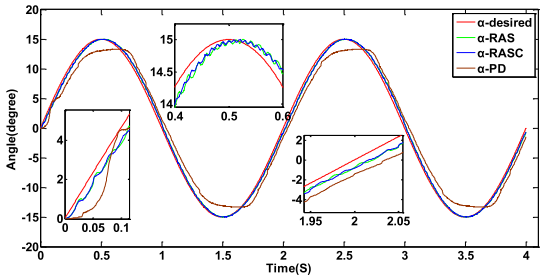

FIGURE 13. Position response to angle α.

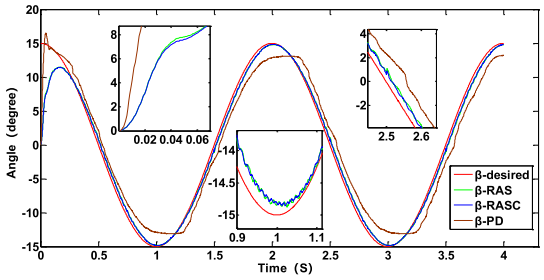

FIGURE 14. Position response to angle β.

The trajectories and errors are shown in Figs. 13 to 15 and Figs. 16 to 18 respectively. The MSEs versus the different angles are shown in Table 2. Compared with the PD controller, the MSEs of RAS in the α, β, γ directions is decreased by 81.2%, 50.4%, and 99.6%, respectively. Compared with the RAS controller, the MSEs of RASC in the α, β, γ directions are reduced by 8.3%, 1.2%, and 25.0% respectively after compensation. Compared with the PD controller, the RAS and RASC controllers respond to large initial error without overshoot, and the convergence rate of error is faster. The experiment results show that the proposed controller can

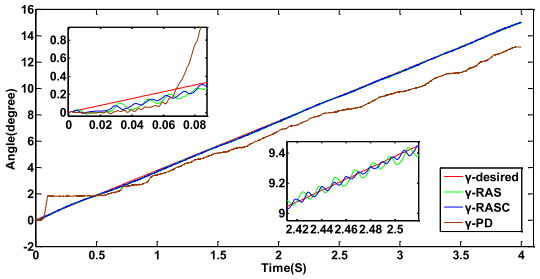

FIGURE 15. Position response to angle γ.

effectively reduce the error caused by friction and uncertain disturbance, and compensate for the Coriolis and centrifugal forces in the output torque. PMSA is controlled to track the desired trajectory. By compensating for the time delay, the tracking error of PMSA can be reduced, thereby improving the tracking accuracy.

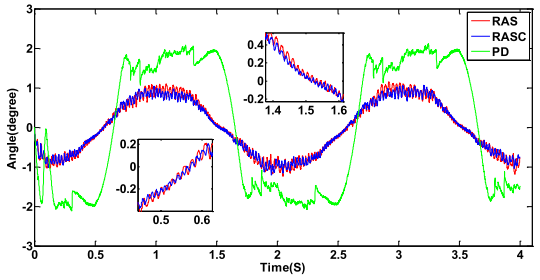

FIGURE 16. Tracking errors versus angle α.

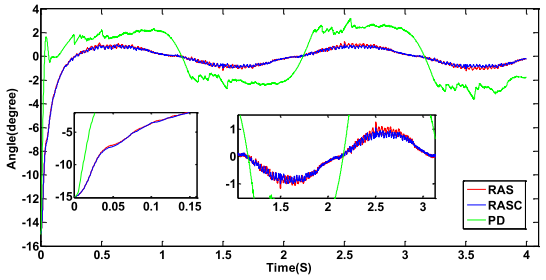

FIGURE 17. Tracking errors versus angle β.

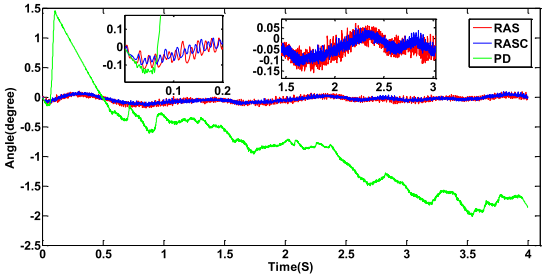

FIGURE 18. Tracking errors versus angle γ.

Apart from performing complex trajectory tracking, PMSA can also be tasked with simple movements such as tilting and spinning. These movements around a single axis can show the effect of inter-axis couplings and how well the effects are compensated by the controller. A typical tilting

TABLE 2. Mean square errors versus the different angle.

Items	PD	RAS	RASC
Errors on angle α	2.6217	0.4933	0.4520
Errors on angle β	4.8760	2.4147	2.3854
Errors on angle γ	1.2795	0.0048	0.0036

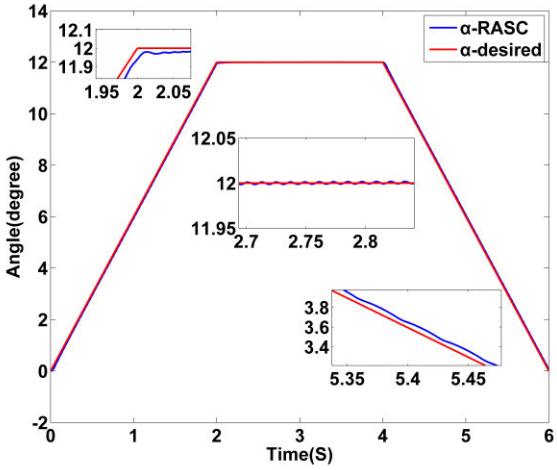

FIGURE 19. Position response to angle α.

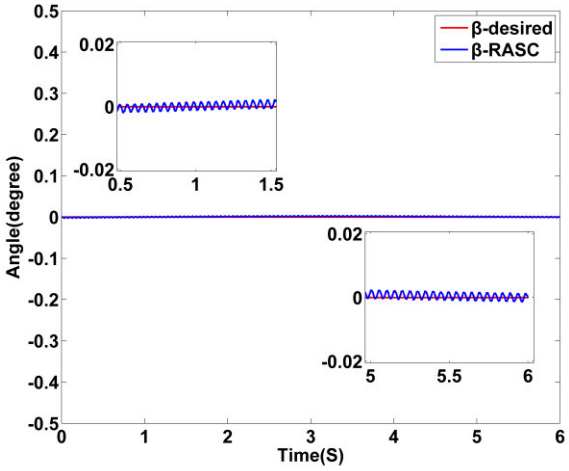

FIGURE 20. Position response to angle β.

motion along the X-axis of rotor is performed to show the performance of the proposed control scheme in dealing with inter-axis couplings. In this experiment, the rotor is controlled to move along the desired trajectory as (34), (35), and the experiment time is set to 6 sec. This desired trajectory is set to be identical with the experiment trajectory in reference [15]. Therefore, this experiment can also be viewed as a reference for comparison with the results of other pertinent works.

$$\begin{cases} \boldsymbol{q}_{\text{des}} = [\alpha(t), 0, 0] \\ \boldsymbol{q}(0) = [0, 0, 0] \end{cases} \tag{34}$$

$$\alpha(t) = \begin{cases} 6t, & t \in [0, 2] \\ 12, & t \in [2, 4] \\ 12 - 6(t-4), & t \in [4, 6] \end{cases} \quad (35)$$

The experiment results are shown in Figs. 19 and 20, indicating that the actual trajectory fits the desired trajectory well under the proposed control scheme. The maximum tracking error measured by sensor is 0.13 degree. Given that the precision of the sensor used in this experiment is 0.05 degree, the real maximum tracking error is between 0.08 and 0.18 degrees. The experimental results illustrate that apart from uncertain disturbances, friction, Coriolis and centrifugal forces, and time delay, the proposed control scheme is also robust against the effects of the inter-axis couplings of α and β.

VII. CONCLUSION

This study proposes an adaptive robust sliding-mode control system with delay compensation is proposed for the trajectory tracking control system of PMSA. The feasibility and efficiency of the proposed method are illustrated by theory and experiments, thereby making it a superior alternative for the sake of providing a solution to PMSA and other industries multi-DOF devices with unknown dynamics. The three main contributions of this research are as follows.

1. An improved LP is proposed, which has superior prediction accuracy when the speed changes rapidly. The delay of the PMSA digital control system is compensated to obtain more accurate position information, which is used as the position signal of the adaptive robust sliding-mode controller.
2. A sliding-mode controller is designed to compensate for the uncertain disturbance of the PMSA control system. Adaptive controller is designed to adapt the parameters of the PMSA online, and the components of Coriolis and centrifugal forces are compensated at the control input to improve the robustness of the entire system.
3. The control strategy proposed in this study combines the improved LP with adaptive robust sliding mode controller, which has good robustness against the inaccuracy of modeling, friction, uncertain disturbance and, computation delay.

Future work will consider the application of extended state observer to compensate for uncertain disturbances, adjustment of controller gains through machine learning, and the chattering issue of sliding-mode controller to acquire an improved control performance.

REFERENCES

[1] K. Bai, R. Xu, K.-M. Lee, W. Dai, and Y. Huang, "Design and development of a spherical motor for conformal printing of curved electronics," *IEEE Trans. Ind. Electron.*, vol. 65, no. 11, pp. 9190–9200, Nov. 2018.
[2] G. Li, H. Li, and B. Li, "Spacecraft attitude maneuver control using two parallel mounted 3-DOF spherical actuators," *Chin. J. Aeronaut.*, vol. 30, no. 1, pp. 419–425, Feb. 2017.
[3] H.-J. Lee, H.-J. Park, S.-H. Won, G.-H. Ryu, and J. Lee, "Improvements of performance of multi-DOF spherical motor by double air-gap feature," *J. Electr. Eng. Technol.*, vol. 8, no. 1, pp. 90–96, Jan. 2013.
[4] K. Bai and K.-M. Lee, "Direct field-feedback control of a ball-joint-like permanent-magnet spherical motor," *IEEE/ASME Trans. Mechatronics*, vol. 19, no. 3, pp. 975–986, Jun. 2014.
[5] H. Son and K.-M. Lee, "Control system design and input shape for orientation of spherical wheel motor," *Control Eng. Pract.*, vol. 24, pp. 120–128, Mar. 2014.
[6] W. Wang, J. Wang, G. W. Jewell, and D. Howe, "Design and control of a novel spherical permanent magnet actuator with three degrees of freedom," *IEEE/ASME Trans. Mechatronics*, vol. 8, no. 4, pp. 457–468, Dec. 2003.
[7] C. Xia, C. Guo, and T. Shi, "A Neural-Network-Identifier and fuzzy-controller-based algorithm for dynamic decoupling control of permanent-magnet spherical motor," *IEEE Trans. Ind. Electron.*, vol. 57, no. 8, pp. 2868–2878, Aug. 2010.
[8] J. Chu, N. Niguchi, and K. Hirata, "Feedback control of outer rotor spherical actuator using adaptive neuro-fuzzy inference system," in *Proc. 7th Int. Conf. Sens. Technol. (ICST)*, Dec. 2013, pp. 401–405.
[9] J. Yao, Z. Jiao, and D. Ma, "Adaptive robust control of DC motors with extended state observer," *IEEE Trans. Ind. Electron.*, vol. 61, no. 7, pp. 3630–3637, Jul. 2014.
[10] J. Yao and W. Deng, "Active disturbance rejection adaptive control of uncertain nonlinear systems: Theory and application," *Nonlinear Dyn.*, vol. 89, no. 3, pp. 1611–1624, Aug. 2017.
[11] Z. Li, "Robust control of PM spherical stepper motor based on neural networks," *IEEE Trans. Ind. Electron.*, vol. 56, no. 8, pp. 2945–2954, Aug. 2009.
[12] Y. Wen, G. Li, Q. Wang, and X. Guo, "Robust adaptive sliding-mode control for permanent magnet spherical actuator with uncertainty using dynamic surface approach," *J. Electr. Eng. Technol.*, vol. 14, no. 6, pp. 2341–2353, Nov. 2019.
[13] H. LI and W. LIU, "Less conservative sliding mode control of permanent magnet spherical motor," *Control Theory Appl.*, vol. 35, no. 2, pp. 137–145, 2018.
[14] X. Guo and Q. Wang, "Adaptive fuzzy control for permanent magnet spherical motor based on friction compensation," *Proc. CSEE*, vol. 31, no. 15, pp. 75–81, May 2011.
[15] J. Liu, X. Li, S. Cai, W. Chen, and S. Bai, "Adaptive fuzzy sliding mode algorithm-based decentralised control for a permanent magnet spherical actuator," *Int. J. Syst. Sci.*, vol. 50, no. 2, pp. 403–418, Jan. 2019.
[16] L. Yang, E. Yu, C.-I. Vong, and L. Zhang, "Discrete-time optimal control of electromagnetic coil systems for generation of dynamic magnetic fields with high accuracy," *IEEE/ASME Trans. Mechatronics*, vol. 24, no. 3, pp. 1208–1219, Jun. 2019.
[17] V. Miskovic, V. Blasko, T. M. Jahns, A. H. C. Smith, and C. Romenesko, "Observer-based active damping of LCL resonance in grid-connected voltage source converters," *IEEE Trans. Ind. Appl.*, vol. 50, no. 6, pp. 3977–3985, Apr. 2014.
[18] D. Pan, X. Ruan, C. Bao, W. Li, and X. Wang, "Capacitor-current-feedback active damping with reduced computation delay for improving robustness of LCL-type grid-connected inverter," *IEEE Trans. Power Electron.*, vol. 29, no. 7, pp. 3414–3427, Jul. 2014.
[19] C. Chen, J. Xiong, Z. Wan, J. Lei, and K. Zhang, "A time delay compensation method based on area equivalence for active damping of an LCL - type converter," *IEEE Trans. Power Electron.*, vol. 32, no. 1, pp. 762–772, Jan. 2017.
[20] Z. Xin, X. Wang, P. C. Loh, and F. Blaabjerg, "Grid-current-feedback control for LCL-filtered grid converters with enhanced stability," *IEEE Trans. Power Electron.*, vol. 32, no. 4, pp. 3216–3228, Apr. 2017.
[21] M. Khazaee, A. H. D. Markazi, and E. Omidi, "Adaptive fuzzy predictive sliding control of uncertain nonlinear systems with bound-known input delay," *ISA Trans.*, vol. 59, pp. 314–324, Nov. 2015.
[22] M. Khazaee, A. H. D. Markazi, S. T. Rizi, and B. Seyfi, "Adaptive fuzzy sliding mode control of input-delayed uncertain nonlinear systems through output-feedback," *Nonlinear Dyn.*, vol. 87, no. 3, pp. 1943–1956, Feb. 2017.
[23] X. Shao, F. Naghdy, H. Du, and H. Li, "Output feedback H_∞ control for active suspension of in-wheel motor driven electric vehicle with control faults and input delay," *ISA Trans.*, vol. 92, pp. 94–108, Sep. 2019.
[24] T. Skovranek, V. Despotovic, and Z. Peric, "Optimal fractional linear prediction with restricted memory," *IEEE Signal Process. Lett.*, vol. 26, no. 5, pp. 760–764, May 2019.
[25] J. Liu, G. Zhai, X. Yang, B. Yang, and L. Chen, "Spatial error concealment with an adaptive linear predictor," *IEEE Trans. Circuits Syst. Video Technol.*, vol. 25, no. 3, pp. 353–366, Mar. 2015.

[26] M. Lu, X. Wang, P. C. Loh, F. Blaabjerg, and T. Dragicevic, "Graphical evaluation of time-delay compensation techniques for digitally controlled converters," *IEEE Trans. Power Electron.*, vol. 33, no. 3, pp. 2601–2614, Mar. 2018.
[27] X. Guo, S. Li, Q. Wang, Y. Wen, and N. Gong, "Dynamic analysis and current calculation of a permanent magnet spherical motor for point-to-point motion," *IET Electr. Power Appl.*, vol. 13, no. 4, pp. 426–434, Apr. 2019.
[28] X. Li, S. Bai, W. Chen, and J. Liu, "Torque modelling and current optimization of a spherical actuator built as an electro-magnets driven spherical parallel manipulator," in *Proc. IEEE Int. Conf. Cybern. Intell. Syst. (CIS) IEEE Conf. Robot., Autom. Mechatronics (RAM)*, Nov. 2017, pp. 626–631.
[29] R. A. Sosseh and K.-M. Lee, "Finite element torque modeling for the design of a spherical motor," in *Proc. 7th Int. Conf. Control, Autom., Robot. Vis. ICARCV*, Dec. 2002, pp. 390–395.

XIWEN GUO graduated from the College of Electrical and Information Engineering, Anhui University of Science and Technology, Huainan, China, in 2005. He received the Ph.D. degree in electrical engineering from the Hefei University of Technology, Hefei, China, in 2012.

He is currently an Associate Professor with Anhui University, Hefei. His research interests include special motor and its control, power electronics and electric drives, intelligent control, and motor-pump modeling.

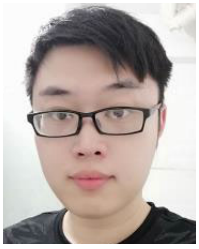

KAIDA PAN received the B.S. degree from the School of Electrical Engineering and Automation, Anhui University, Hefei, China, in 2018, where he is currently pursuing the M.S. degree.

His current research interest includes control strategy of permanent magnet spherical actuator.

QUNJING WANG received the Ph.D. degree from the University of Science and Technology of China, Hefei, China, in 1998.

He is currently a Professor and a Ph.D. Tutor with the Industrial Energy Saving and Power Quality Control of Collaborative Innovation Center, Anhui University, Hefei. His research interests include electrical machines, motor drives, and new electric drive systems.

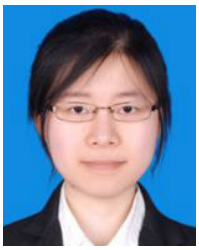

YAN WEN is currently pursuing the Ph.D. degree with the School of Electrical Engineering and Automation, Anhui University, China. Her research interests include novel spherical actuator and its control and orientation measurement and complex system modeling and analysis.